Geol. Mag. **145** (*3*), *2008, pp. 305–320. © 2008 Cambridge University Press*
doi:10.1017/S0016756807004311 *Printed in the United Kingdom*

A Jurassic peraluminous leucogranite from Yiwulüshan, western Liaoning, North China craton: age, origin and tectonic significance

XIAO-HUI ZHANG*†‡, QIAN MAO*, HONG-FU ZHANG* & SIMON A. WILDE†

*State Key Laboratory of Lithospheric Evolution and Key Laboratory of Mineral Resources, Institute of Geology and Geophysics, Chinese Academy of Sciences, Beijing 100029, China
†Department of Applied Geology, Curtin University of Technology, Perth WA, Australia

(*Received* 24 April 2007; *accepted* 26 June 2007; First published online 28 January 2008)

Abstract – The Gangjia granite stock is a garnet-bearing muscovite leucogranitic body emplaced in Yiwulüshan in Western Liaoning Province at the eastern segment of the Yanshan orogenic belt, North China craton. The SHRIMP U–Pb zircon age is 153 ± 5 Ma. The Gangjia granites are peraluminous with A/CNK of more than 1.14, and exhibit a tetrad effect in their REE distribution patterns, as well as non-charge-and-radius-controlled trace element behaviour. This is in contrast to the LREE-enriched patterns of the host Lüshan monzogranites. These geochemical characteristics, together with low Th/U ratios in zircon, suggest that the parental magmas for the Gangjia granites have experienced extensive magmatic differentiation, including interaction between residual melt and a coexisting high-temperature aqueous fluid. Their similar $\varepsilon_{Nd}(t)$, model ages, compatible age patterns and common volcanic arc signature in source materials between the Gangjia granites and the host Lüshan monzogranites indicate their comagmatic relationship. These unusual peraluminous leucogranites, coupled with the voluminous adakitic granites hosting them, represent typical post-orogenic magmatism developed under an intra-continental extensional tectonic regime. At the very end of the prolonged Jurassic magmatic evolution in Western Liaoning, extensive fractionation of most probably ferromagnesian phases and plagioclase from a calc-alkaline magma parental to the host Lüshan pluton, with overprint of the magmatic hydrothermal fluid, produced highly evolved peraluminous parental magmas for the Gangjia granites.

Keywords: leucogranite, geochemistry, petrogenesis, North China craton.

1. Introduction

Peraluminous leucogranites form a small but genetically important component of granitic intrusions in most orogenic belts of various ages (e.g. Barbarin, 1996; Williamson *et al.* 1996; Nabelek & Bartlett, 1998; Frost *et al.* 2001). Numerous studies on various types of peraluminous leucogranites worldwide reveal that they are genetically diverse and can be produced from various sources and through different evolutionary processes (e.g. Frost *et al.* 2001). Given the fact that the only consistent features they share are their high silica content and strongly peraluminous nature, any attempt at classifying them as one specific type under any genetic or tectonic geochemical classification schemes seem unlikely. However, applying an additional constraint like REE tetrad patterns, such peraluminous leucogranites can be useful geodynamic tracers, due to their similar characteristics to A-type granitoids and their consistent occurrence within a post-orogenic extensional tectonic setting (Sibel, Hohndorf & Wendt, 1995; Williamson *et al.* 1996; Förster *et al.* 1999; Monecke *et al.* 2002; Jahn *et al.* 2001, 2004*a*; Wu *et al.* 2004; Sun *et al.* 2005). Their recognition may allow the determination of the tectonic setting of ancient orogens.

The Yiwulüshan range lies in Western Liaoning Province, which constitutes the eastern segment of the Yanshan orogenic belt in the North China craton (Fig. 1a, b). It is occupied by voluminous Mesozoic granitoid plutons (Fig. 1c). Recent zircon U–Pb geochronological studies focusing on Yiwulüshan and Western Liaoning (Wu, Yang & Zhang, 2006) indicate that the Yiwulüshan batholiths were mainly emplaced during middle to late Jurassic times. Geochemically, the Yiwulüshan granitoids display many close compositional similarities to high-silica adakites (Liu *et al.* 2002). In this paper, we present new age, geochemical and Sr–Nd isotopic data for a peraluminous leucogranite pluton, the Gangjia stock, that intruded into the Lüshan pluton from the Yiwulüshan batholiths (Fig. 1d). The stock shows spectacular tetrad-like REE patterns and other non-charge-and-radius-controlled trace elements. Zircon U–Pb SHRIMP dating shows a late Jurassic emplacement time. The first documentation of such unusual magmatism in Yiwulüshan carries important implications for further constraining the controversial tectonic setting of the prolonged Jurassic magmatism in Western Liaoning.

‡Author for correspondence: zhangxh@mail.iggcas.ac.cn

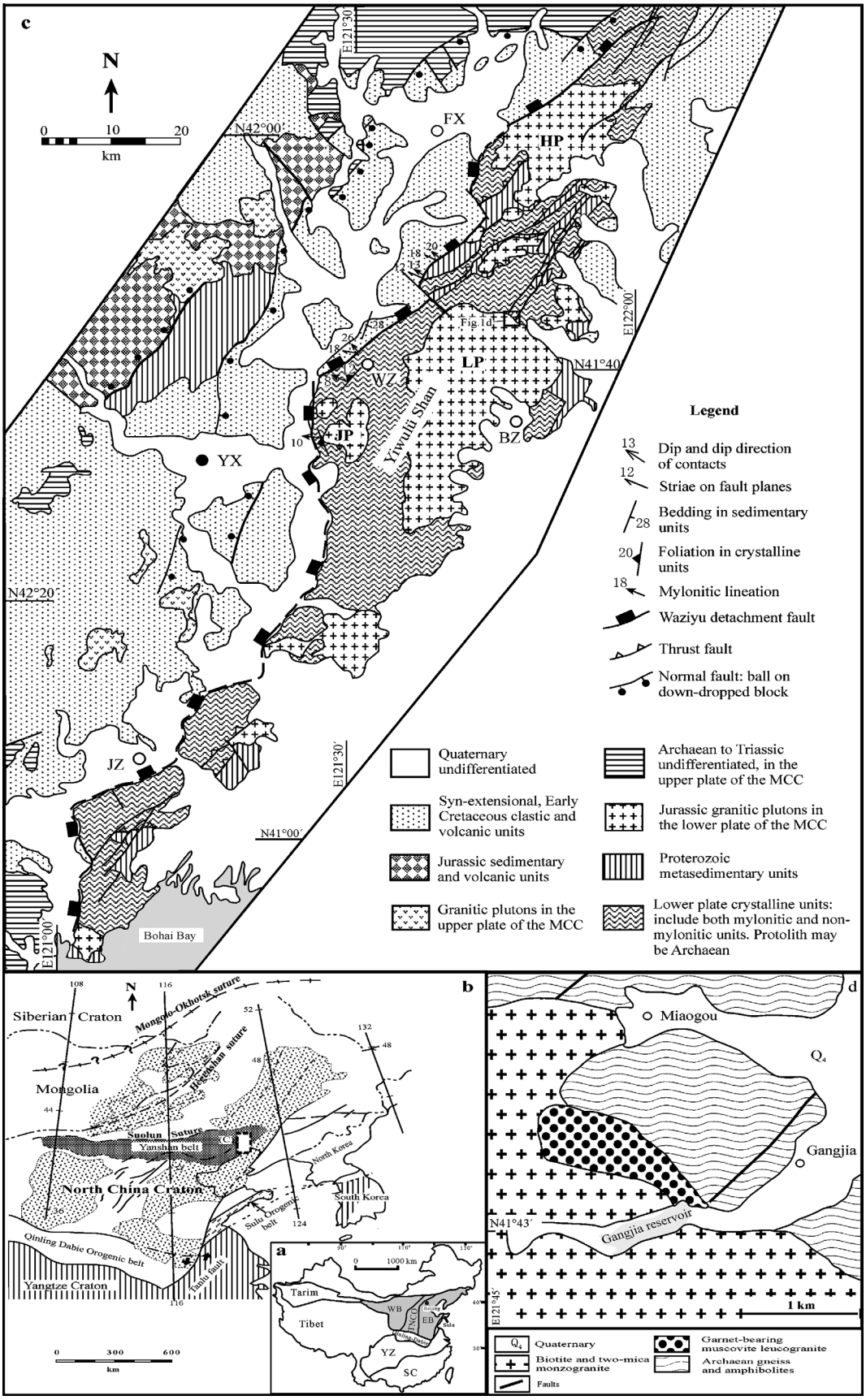

Figure 1. (a) Major tectonic divisions of China, where YZ and SC denote the Yangtze craton and South China orogen. Also shown are the subdivisions of the North China craton (Zhao *et al.* 2001), where EB, TNCO and WB denote the Eastern block, Trans-North China orogen and Western block, respectively. (b) Simplified geological map showing the major tectonic units of the North China craton and its surrounding areas, with the study area indicated by a rectangle (modified from Davis *et al.* 2001). Stippled fields denote the

https://doi.org/10.1017/S0016756807004311 Published online by Cambridge University Press

2. Geological setting

The Yanshan belt is located along the northern margin of the North China craton (Fig. 1a, b), which is bounded on the south by the Palaeozoic to Triassic Qinling–Dabie–Sulu orogenic belt (Meng & Zhang, 2000) and on the north by the Central Asian Orogenic Belt (Davis *et al.* 2001).

As evidenced by the presence of ≥ 3.6 Ga crustal remnants exposed at the surface or in the lower crustal xenoliths (Liu *et al.* 1992; Zheng *et al.* 2004), the North China craton has been regarded as one of the world's oldest cratons. It consists of two Archaean continental blocks, namely, the Eastern and the Western, separated by a Proterozoic orogenic belt (Fig. 1a; Zhao *et al.* 2001). The basement of the North China craton is composed of amphibolite to granulite facies Archaean grey tonalitic gneisses and greenstones and Palaeoproterozoic khondalites and an overlying unmetamorphosed sedimentary cover from the Mesoproterozoic onwards (Zhao *et al.* 2001, 2005). It was widely believed that the Eastern and Western Blocks developed independently from the late Archaean to early Palaeoproterozoic and collided to form a coherent craton at *c.* 1.85 Ga (Zhao *et al.* 2001, 2005).

Unlike other Archaean cratons, the North China craton experienced widespread tectonothermal reactivation during and after the Palaeozoic, mainly due to the compound evolutionary history of the circum-cratonic orogenic belts. To the north of the craton, the generally EW-trending Central Asian Orogenic Belt was formed through south-directed subduction and arc–arc, arc–continent, and continent–continent collision, mainly during the Palaeozoic (Davis *et al.* 2001; Xiao *et al.* 2003). During this time, multiple Ordovician to Permian oceanic arcs and the Mongolian micro-continent were amalgamated to the active margins of the North China craton (Davis *et al.* 2001). The widespread occurrence of Palaeozoic ophiolites, Palaeozoic to Triassic blueschists, and synchronous igneous rocks suggest that southward subduction commenced in the early Palaeozoic and that collision was completed in the early Triassic (Davis *et al.* 2001, 2004; Buchan *et al.* 2002). The Solonker suture records the termination of the Central Asian Orogenic Belt (Xiao *et al.* 2003). With the gradual exhaustion of the palaeo-Asian Ocean Realm (Wang & Mo, 1995), the North China block and the southern Mongolia terranes were amalgamated and behaved as a combined North China–Mongolian plate (Davis *et al.* 2001).

Following early Mesozoic crustal extension of still uncertain origin (Meng, 2003), as documented by the synchronous occurrence of alkali igneous intrusions (Yan *et al.* 2000), late Triassic metamorphic core complexes (Davis *et al.* 2004) and early Jurassic rifted basins (Ritts, Darby & Cope 2001), the North China–Mongolian plate became the locus of the Yanshanian orogeny during middle Jurassic to earliest Cretaceous time, in response to the continental collision of Siberia and the North China–Mongolian plate along the Mongol–Okhotsk suture (Yin & Nie, 1996; Zorin, 1999). The resulting fold-thrust deformation is well-documented in the Yanshan belt (Davis *et al.* 1998, 2001). Subsequent to this period of crustal shortening, another intensive extensional deformation developed in the North China–Mongolian plate during early Cretaceous time, as manifested by development of extensional basins and metamorphic core complexes, and widespread alkali volcanism and plutonism (Meng, 2003, and references therein).

Western Liaoning represents the eastern segment of the Yanshan belt and experienced a complex history during Mesozoic time. Middle Jurassic contractional deformation is evidenced by well-developed thin-skinned thrusts (Davis *et al.* 2001; Zhang *et al.* 2002). In the Cretaceous, the area underwent extensional deformation, resulting in the development of a number of rift-related basins (e.g. the Fuxin basin: Xu *et al.* 2000), the Waziyu metamorphic core complex (Zhang, Wang & Ma, 2003; Darby *et al.* 2004) and widespread alkali volcanism (Zhang *et al.* 2003).

As shown in Figure 1c, the Waziyu metamorphic core complex has an east–west dimension of 25 km and a north–south dimension of 60 km. The core consists predominantly of Mesozoic granitoid plutons and their country rocks, which include high- to medium-grade migmatitic orthogneiss and amphibolites of the Archaean crystalline basement. Plutons are granodioritic to granitic and grade outward into augen gneiss or migmatite. At structurally higher levels is the well-developed NNE-trending Waziyu ductile shear zone that, together with the related normal fault above it along the eastern margin of the Fuxin basin, separates the core of the dome (the lower plate) from the upper plate of the unmetamorphosed to low-grade metamorphosed middle–late Proterozoic Changcheng System and the Mesozoic volcano-sedimentary rocks.

As compiled by Wu, Yang & Zhang (2006), Mesozoic intrusions from Western Liaoning appear to occur in four episodes: the first episode of rare Triassic dioritic magmatism (221 ± 2 Ma); the second

Mesozoic sedimentary basins. Dashed lines within the Mesozoic sedimentary basins are the trends of Jurassic–Cretaceous extensional faults. Between the Suolun Suture and the Mongolo–Okhotsk suture is the Central Asian Orogenic Belt. (c) Simplified tectonic map of the Yiwulüshan, western Liaoning province (adopted from Darby *et al.* 2004), showing major structures and plutons. LP – Lüshan pluton; JP – Jianlazishan pluton; HP – Hengshan pluton. BZ – Beizhen; FX – Fuxin; YX – Yixian; JZ – Jinzhen; WZ – Waziyu. MCC – metamorphic core complex. (d) Geological sketch map of the Gangjia leucogranitic stock (modified from LBGMR, 1998).

https://doi.org/10.1017/S0016756807004311 Published online by Cambridge University Press

and third episodes of voluminous granitic magmatism represented by the Jurassic Jianchang (175–190 Ma) and Yiwulüshan batholiths respectively; and the fourth episode of the limited early Cretaceous granitic magmatism. Therefore, Middle to late Jurassic times saw the most voluminous plutonism in Western Liaoning.

As part of this voluminous magmatism, the Lüshan pluton crops out in the core of the Yiwulüshan as a north–northeast elongate dome (Fig. 1c) and covers an area of over 250 km^2. The pluton is mainly composed of monzogranite and granodiorite. For the age of this composite pluton, we obtained a TIMS zircon U–Pb age of 164 ± 9 Ma (Zhang *et al.* unpub. data). Wu, Yang & Zhang (2006) also reported two zircon U–Pb ages based on the LA-ICPMS method: a monzogranite sample yields an emplacement age of 163 ± 3 Ma ($n = 11$) and an inherited age of 206 ± 4 Ma ($n = 2$), while another granodiorite sample gives an emplacement age of 153 ± 2 Ma ($n = 14$) and two inherited ages of 216 ± 7 Ma ($n = 7$) and 187 ± 6 Ma ($n = 6$). The pluton bears a remarkable geochemical resemblance to the high-silica adakites, such as low abundances of garnet-compatible elements (Y and HREE), high contents of plagioclase-compatible Sr and Ba, high ratios of Sr/Y and La/Yb, absence of significant Eu anomalies, and concave-upward shapes of chondrite-normalized HREE patterns (Liu *et al.* 2002).

3. Petrology

The Gangjia granite stock, named after Gangjia village, is exposed near the Gangjia reservoir and intrudes the Lüshan pluton (LBGMR, 1998) (Fig. 1d). It is mainly composed of garnet-bearing muscovite leucogranite, including near-equigranular granite (samples FX18-20 and LX13-14) and microgranite with very fine-grained matrix and phenocrysts (samples FX11-1 to FX11-8). The mineral assemblage includes quartz (30–40 %), alkali-feldspar (30–55 %), albite (5–20 %), muscovite (1–8 %) and garnet (1–5 %). Quartz is present both as rounded phenocrysts and as small grains in the matrix. K-feldspar phenocrysts are commonly rounded and partially or totally exsolved into microcline. Albite commonly occurs as euhedral to subhedral laths, but it also forms small anhedral grains in the matrix of microgranites. Primary muscovite is present as large anhedral crystals and commonly found between quartz and feldspar grains, but never occurs as inclusions within them. Secondary symplectic muscovite is locally found in the matrix of microgranites. Garnet occurs both as large anhedral interstitial grains in the granites and small euhedral grains in the matrix of microgranites. It also occasionally occurs as inclusions within phenocrysts of K-feldspar and albite. The presence of primary muscovite and magmatic garnet and absence of biotite indicate the highly fractionated nature of the rocks.

4. Analytical techniques

Zircons were separated using conventional heavy liquid and magnetic techniques and by hand-picking under a binocular microscope. Zircon U–Pb analyses were performed using the Sensitive High-Resolution Ion Microprobe (SHRIMP II) at the Institute of Geology, Chinese Academy of Geological Sciences, Beijing. Zircons, together with grains of the Temora zircon standard (TEM: see Black *et al.* 2003), were mounted in epoxy and the grains sectioned by grinding and polishing. Zircons were studied using transmitted and reflected light photographs and cathodoluminescence (CL) images at the Institute of Geology and Geophysics, Chinese Academy of Sciences (IGGCAS), and the mount was vacuum-coated with a 50 nm layer of high-purity gold. Detailed analytical procedures are similar to those described by Williams (1998). Interelement fractionation in ion emission of zircon was corrected relative to the RSES references, using SL13 (572 Ma, 238 ppm) for the final calibration. Due to the small amount of ^{207}Pb present in young zircons, which results in low count rates and high analytical uncertainties, the ^{206}Pb/^{238}U ratios are generally considered to be the most reliable for concordant Phanerozoic zircons (Compston *et al.* 1992). The SHRIMP analytical data presented in Table 1 are the mean values of five cycle analyses of each zircon spot. Data were processed using SQUID (1.02) and ISOPLOT (Ludwig, 2001). The common Pb corrections were made using the measured ^{204}Pb. Uncertainties quoted in the data table are $\pm 1\sigma$, whereas the weighed mean ages are quoted at $\pm 2\sigma$.

For elemental and isotopic analyses, samples were ground in an agate mill to ~ 200 mesh. Major oxides were analysed using a Phillips PW 2400 X-ray fluorescence spectrometer (XRF) and the trace element abundances were obtained on a VG-PQII ICP-MS at IGGCAS. Samples were dissolved in distilled $HF + HNO_3$ in 15 ml Savillex Teflon screw-cap beakers at 120 °C for six days, dried and then diluted to 50 ml for analysis. A blank solution was prepared and the total procedural blank was < 50 ng for all trace elements. Indium was used as an internal standard to correct for matrix effects and instrument drift. Analytical uncertainty (2σ) is estimated to be ± 5 % for trace elements with abundances ≥ 10 ppm, and ca. ± 10 % for those ≤ 10 ppm.

For Sr–Nd isotopic analyses, sample powders were dissolved in Teflon bombs after being spiked with ^{84}Sr, ^{87}Rb, ^{150}Nd and ^{147}Sm tracers prior to $HF + HNO_3$ dissolution. Rb, Sr, Sm and Nd were separated using conventional ion exchange procedures and measured using a Finnigan Mat 262 multicollector mass spectrometer at IGGCAS. Procedural blanks were < 100 pg for Sm and Nd and < 500 pg for Rb and Sr. ^{143}Nd/^{144}Nd were corrected for mass fractionation by normalization to ^{146}Nd/^{144}Nd $= 0.7219$, and ^{87}Sr/^{86}Sr ratios normalized to ^{86}Sr/^{88}Sr $= 0.1194$. Repeated analyses yielded

https://doi.org/10.1017/S0016756807004311 Published online by Cambridge University Press

Table 1. SHRIMP U–Pb zircon data for the Gangjia leucogranites

Spot	U (ppm)	Th (ppm)	Th/U	Pb (ppm)	f_{206} [1] (%)	$^{207}Pb/^{206}Pb$ (± % error 1σ)	$^{206}Pb/^{238}U$ (± % rror 1σ)	$^{207}Pb/^{235}U$ (± % error 1σ)	Error correlation	Age (Ma) $^{206}Pb/^{238}U \pm 1\sigma$
FX18-1	2443	186	0.08	50.5	0.22	0.0492 ± 3	0.02403 ± 2	0.1630 ± 4	0.756	153 ± 3
FX18-2	2102	145	0.07	44.1	0.7	0.0505 ± 3	0.02425 ± 2	0.1690 ± 4	0.741	154 ± 3
FX18-3	1855	222	0.12	38.9	0.29	0.0517 ± 2	0.02436 ± 2	0.1738 ± 3	0.728	155 ± 3
FX18-4	2278	197	0.09	50.4	0.5	0.0496 ± 2	0.02563 ± 2	0.1753 ± 3	0.725	163 ± 3
FX18-6	310	200	0.67	7.9	0.8	0.0514 ± 6	0.02933 ± 2	0.2080 ± 5	0.48	186 ± 5
FX18-7	1854	233	0.13	41.9	0.32	0.0494 ± 3	0.02623 ± 2	0.1787 ± 4	0.585	167 ± 4
FX18-9	822	889	1.12	17	1.95	0.0469 ± 3	0.02361 ± 2	0.1527 ± 4	0.524	150 ± 4
FX18-10	1736	121	0.07	36.3	0.39	0.0468 ± 3	0.02427 ± 2	0.1565 ± 3	0.686	155 ± 3
FX18-11	3768	244	0.07	82.4	0.14	0.0494 ± 1	0.02541 ± 2	0.1730 ± 3	0.825	162 ± 3
FX18-12	2338	180	0.08	61.9	2.03	0.0503 ± 3	0.03019 ± 2	0.2095 ± 3	0.626	192 ± 4

[1] f_{206} = percentage of common ^{206}Pb in the total measured ^{206}Pb.

$^{87}Sr/^{86}Sr$ of 0.710253 ± 0.000015 for the NBS-987 standard and $^{143}Nd/^{144}Nd$ of 0.5511853 ± 0.000009 for the La Jolla standard. The decay constants used in age computation are $^{87}Rb = 0.0142\ Ga^{-1}$ and $^{87}Sm = 0.00654\ Ga^{-1}$.

Sm–Nd model ages were calculated in two ways. The one-stage model age (T_{DM1}) is calculated assuming a linear Nd isotopic growth of the depleted mantle reservoir from $\varepsilon_{Nd} = 0$ at 4.56 Ga to $\varepsilon_{Nd} = +10$ at the present:

$$T_{DM1} = 1/\lambda\ \ln\{1 + [(^{143}Nd/^{144}Nd)_{sample}] - 0.51315\}/ [(^{147}Sm/^{144}Nd)_{sample} - 0.21317],$$

where s = sample and λ = decay constant of ^{147}Sm ($0.00654\ Ga^{-1}$).

Since T_{DM1} ages depend strongly on the $^{147}Sm/^{144}Nd$ ratios, the highly fractionated nature of the Gangjia granites has resulted in increasing Sm/Nd and thus caused inaccurate and diverse T_{DM1} ages (Table 3). Therefore, we adopt a refined equation similar to that of Liu *et al.* (2005) for calculating the depleted mantle model age, T_{DM2}, instead of T_{DM1}:

$$T_{DM2} = 1/\lambda \times \ln\{1 + [(^{143}Nd/^{144}Nd)_{sample} - (e^{\lambda t} - 1) \times [(^{147}Sm/^{144}Nd)_{sample} - (^{147}Sm/^{144}Nd)_s] - (^{143}Nd/ \times {}^{144}Nd)_{DM}]/[(^{147}Sm/^{144}Nd)_s - (^{147}Sm/^{144}Nd)_{DM}]\}$$

where the subscripts S and DM refer to the source rock and the depleted mantle, respectively, and t is the emplacement age of the granite stock. The lowest $^{147}Sm/^{144}Nd$ value was chosen from the samples to represent the $(^{147}Sm/^{144}Nd)_s$ value in order to offset Sm/Nd fractionation to a minimum.

5. Results

5.a. Geochronology

Zircons from sample FX18 are light yellow, 40–110 μm in length (length/width ratios between 3:1 and 1.5:1), transparent and locally with few inclusions and fractures (Fig. 2a). They are mostly sub-euhedral columnar crystals. Because of the rarity and small size of zircons, we only managed to conduct analysis on ten zircons. As shown in Figure 2b, the main population comprises five analyses forming a nearly concordant group and has a weighted mean age of 153 ± 5 Ma with an MSWD of 0.07. This age is taken to represent the crystallization age of the Gangjia stock. In addition, the other five analyses of zircons give two inherited concordant ages of 191 ± 8 Ma (n = 2) and 162 ± 1 Ma (n = 3) (Fig. 2b), which are consistent with the inherited and emplacement ages of the host Lushan pluton, respectively.

https://doi.org/10.1017/S0016756807004311 Published online by Cambridge University Press

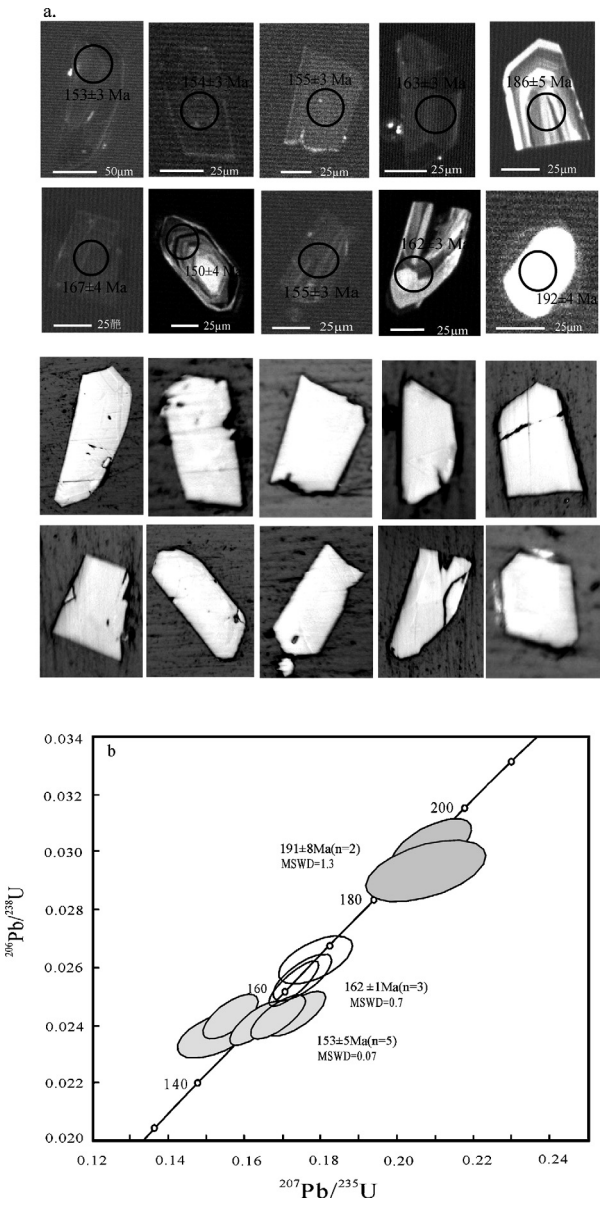

Figure 2. (a) Cathodoluminescence (CL) and transmitted light (TL) images of the dated zircons and (b) SHRIMP U–Pb isotope analyses of zircons from the Gangjia leucogranites.

5.b. Major and trace element chemistry

Major and trace element compositions of the Gangjia stock are given in Table 2. The Gangjia granites are highly siliceous with a narrow SiO_2 range from 74.86 to 75.82 %. They have relatively high contents of alkalis, with total $K_2O + Na_2O$ varying from 7.96 to 8.51 %. They have low abundances of Fe_2O_{3t} (0.26–0.63 %), MnO (0.07–0.17 %), MgO (0.05–0.13), CaO (0.29–0.53), TiO_2 (0.04–0.06 %) and P_2O_5 (< 0.1 %), while Al_2O_3 contents range from 13.9 % to 14.8 %. Their bulk composition shows a strongly peraluminous character with A/CNK > 1.14.

In terms of trace elements, the Gangjia granites are characterized by low abundance in Ba and Sr, high Rb/Sr ratios and high concentrations in Ga, Nb, Ce and Y. Their 10 000 × Ga/Al ratios range from 2.97 to 3.54, which are slightly lower than the global average of 3.75 for A-type granites (Whalen, Currie & Chappell, 1987), but comparable to the aluminous A-type granites in NE China (e.g. Wu *et al.* 2002). In the discrimination diagrams of Whalen, Currie & Chappell (1987), the Gangjia granites plot on the A-type granite field in the $K_2O + Na_2O$ v. 10 000 Ga/Al diagram (Fig. 3a), but on the fractionated felsic I-type granite field in the $(K_2O + Na_2O)/CaO$ v. (Zr + Nb + Ce + Y) diagram (Fig. 3b). In the Nb v. Y and Rb v. Y + Nb tectonic discriminator diagrams of Pearce, Harris & Tindle (1984) (Fig. 3c, d), they plot in the VAG (volcanic arc granite) field and also exclusively fall in the post-collisional field of Pearce (1996), which suggests the beginning of the transition from calc-alkaline to alkaline magmatic series in orogenic to post-orogenic tectonic settings (Barbarin, 1999).

Chondrite-normalized REE patterns are shown in Figure 4a. All the samples show REE tetrad patterns with large negative Eu anomalies ($Eu/Eu^* = 0.10$–0.35; Table 2), similar to the Woduhe and Dongqing leucogranites from the Central Asian Orogenic belt (Jahn *et al.* 2001; Wu *et al.* 2004), but in contrast with the LREE-enriched patterns displayed by the high Sr/Y monzogranites from the host Lüshan pluton. In all individual patterns, four elemental groups (La–Nd, Nd–Ga, Gd–Er, Er–Lu) form four distinct convex patterns. This is the characteristic REE tetrad pattern, well demonstrated in highly differentiated rocks with strong hydrothermal interactions (Jahn *et al.* 2001). In the primitive-mantle-normalized spidergrams (Fig. 4b), the Gangjia granites show enrichment in Rb, Th, U, K and Pb, but strong depletion in Ba, Sr, P, Eu and Ti.

5.c. Sr and Nd isotopic data

The results of Sr–Nd isotope analyses are given in Table 3. The initial isotopic ratios were calculated based on the age of 153 Ma. As shown in a plot of $\varepsilon_{Nd}(T)$ versus $(^{87}Sr/^{86}Sr)_i$ (Fig. 5), the Gangjia granites have strongly negative $\varepsilon_{Nd}(t)$ values (−13.8 to −19.4) and a rather large range of initial $^{87}Sr/^{86}Sr$ ratios, from 0.6875 to 0.7124. Such a large variation in these age-corrected ratios is probably due to the very high $^{87}Rb/^{86}Sr$ ratios of the rocks (Jahn *et al.* 2001). As has been widely suggested, initial $^{87}Sr/^{86}Sr$ values for such high Rb/Sr rocks should not be used in petrogenetic discussions (e.g. Jahn *et al.* 2001). The samples show a large range of T_{DM1} because of the variation of $f_{Sm/Nd}$ resulting from the REE tetrad effect. Using the refined model, the resultant model ages (T_{DM2}) would have a meaningful range from 2183 to 2276 Ma, with the exception of the sample FX-20, which has a lower model age of 1864 Ma (Table 3). This range of model ages is similar to that (2.2–2.4 Ga: Zhang *et al.* unpub. data) for the host Lüshan monzogranites.

https://doi.org/10.1017/S0016756807004311 Published online by Cambridge University Press

Table 2. Major and trace element data for the Gangjia leucogranites

Sample no.	FX11-1	FX11-2	FX11-4	FX11-5	FX11-8	FX18	FX19	FX20	LX-13[1]	LX-14[1]
SiO_2	75.21	75.35	75.74	75.82	75.28	74.87	74.86	75.48	75.62	75.43
TiO_2	0.04	0.05	0.04	0.04	0.04	0.06	0.06	0.05	0.05	0.04
Al_2O_3	14.35	14.3	14.47	13.88	14.44	14.83	14.79	14.2	14.19	14.11
TFe_2O_3	0.44	0.53	0.48	0.55	0.39	0.63	0.63	0.4	0.47	0.26
MnO	0.13	0.11	0.07	0.17	0.11	0.14	0.14	0.1	0.11	0.12
MgO	0.09	0.1	0.09	0.09	0.09	0.14	0.12	0.09	0.13	0.05
CaO	0.53	0.45	0.44	0.52	0.51	0.29	0.29	0.32	0.33	0.29
Na_2O	4.35	4.24	4.39	4.09	4.33	4.08	4.13	4.01	4.01	3.64
K_2O	4.16	4.03	4.08	4.1	4.17	4.37	4.38	4.47	4.19	4.32
P_2O5	0.03	0.03	0.03	0.03	0.04	0.06	0.06	0.04	0.04	0.04
LOI	0.52	0.57	0.58	0.47	0.61	0.75	0.77	0.61	0.81	1.06
Total	99.86	99.76	100.41	99.76	100.01	100.22	100.23	99.68	99.95	99.36
A/CNK	1.15	1.18	1.16	1.15	1.15	1.26	1.25	1.18	1.21	1.26
A/NK	1.24	1.27	1.25	1.25	1.24	1.29	1.29	1.23	1.26	1.33
Sc	1.35	1.98	1.73	1.41	1.69	3.18	3.98	2.27	2.31	2.19
V	1.98	3.46	2.55	3.11	2.03	2.67	5.09	1.89	2.16	0.94
Co	0.1	0.08	0.07	0.13	0.12	0.13	0.95	0.17	0.16	0.16
Zn	9	7.61	7.5	10.35	11.3	11.94	11.46	14.4		
Ga	22.57	25.93	24.95	22.72	25.87	28.28	27.69	24.21	24.59	22.96
Rb	157.2	154.9	160.5	152.7	155.7	211	204.5	183.5	167.5	185
Sr	36.53	21.29	15.88	43.05	31.21	18.77	26.61	21.32	18.6	33.2
Y	13.43	15.22	12.9	13.32	13.27	10.57	11.28	9.75	10.64	8.57
Zr	30.22	28.88	23.14	32.61	31.56	25.35	26.04	23.25	19.39	22.54
Nb	17.38	22.23	20.53	17.51	24.34	29.04	27.92	21	22.97	31.29
Cs	1.01	0.98	1.04	0.89	0.99	1.08	1.51	1.34	0.95	1.07
Ba	27.95	12.19	6.64	42.51	23.21	47.25	7.96	54.56	40.94	87.26
Hf	1.8	1.99	1.65	1.93	1.97	2.01	1.81	1.85	1.47	2
Ta	1.48	1.81	1.47	1.73	2.04	2.97	2.56	2.05	2.16	2.27
Pb	17.74	18.6	17.28	17.28	18.49	13.79	13.26	20.64	11.46	12.94
Th	1.68	1.95	2.17	1.23	1.66	1.39	1.54	1.14	1.09	1.06
U	0.58	0.91	0.74	0.52	0.59	0.74	0.73	1.28	0.7	0.59
La	3.49	3.92	3.97	2.79	2.88	2.8	3.43	2.71	2.36	2.05
Ce	8.03	9.56	9.67	6.3	6.79	6.62	7.91	6.93	6.14	5.54
Pr	1.03	1.22	1.26	0.78	0.98	0.93	1.06	0.94	0.77	0.69
Nd	4.08	5.06	5.17	3.15	3.56	3.82	4.46	3.55	2.85	2.53
Sm	1.18	1.45	1.46	0.94	1.21	1.17	1.32	1.14	1.01	0.94
Eu	0.12	0.08	0.06	0.12	0.07	0.04	0.09	0.05	0.05	0.04
Gd	1.42	1.68	1.6	1.24	1.49	1.26	1.37	1.17	1.24	1
Tb	0.3	0.35	0.32	0.29	0.32	0.26	0.27	0.23	0.29	0.21
Dy	2.02	2.44	2.1	2.05	2.05	1.75	1.81	1.53	1.76	1.5
Ho	0.45	0.52	0.44	0.46	0.42	0.36	0.37	0.29	0.33	0.29
Er	1.27	1.45	1.26	1.33	1.16	1.04	1.1	0.81	1.04	0.81
Tm	0.19	0.22	0.19	0.21	0.18	0.16	0.19	0.12	0.17	0.13
Yb	1.16	1.4	1.14	1.31	1.12	0.99	1.21	0.79	1.14	0.88
Lu	0.17	0.21	0.17	0.19	0.18	0.14	0.17	0.12	0.14	0.11
La_N/Yb_N	2.16	2.01	2.5	1.53	1.84	2.03	2.04	2.46	1.48	1.67
Eu/Eu*	0.28	0.15	0.12	0.35	0.16	0.1	0.2	0.13	0.14	0.13
Ga/Al	2.97	3.43	3.26	3.09	3.42	3.6	3.54	3.22	3.27	3.07
K/Rb	220	216	211	223	222	211	178	202	208	194
K/Ba	1235	2743	5099	800	1491	767	4566	680	849	398
Zr/Hf	16.8	14.5	14	16.9	16	12.6	14.4	12.6	13.2	11.3
Nb/Ta	11.74	12.28	13.97	10.12	11.93	9.78	10.91	10.24	10.63	13.78
La/Nb	0.2	0.18	0.19	0.16	0.12	0.1	0.12	0.13	0.1	0.07
La/Ta	2.36	2.17	2.7	1.61	1.41	0.94	1.33	1.32	1.09	0.9
Sr/Eu	304	266	265	359	446	469	296	426	372	830
Y/Ho	29.8	29.3	29.3	29	31.6	29.4	30.5	33.6	32.2	29.6
Ce*	1.06	1.09	1.08	1.05	1.07	1.04	1.03	1.13	1.19	1.22
Pr*	1.04	1.03	1.04	1.01	1.16	1.06	1.02	1.14	1.13	1.15
TE_1	1.05	1.06	1.06	1.03	1.11	1.05	1.02	1.13	1.16	1.18
Tb*	1.12	1.15	1.11	1.18	1.19	1.13	1.1	1.13	1.32	1.15
Dy*	1.05	1.09	1.06	1.1	1.1	1.1	1.08	1.14	1.18	1.17
TE_3	1.08	1.12	1.09	1.14	1.14	1.11	1.09	1.13	1.25	1.16
$TE_{1,3}$	1.07	1.09	1.07	1.08	1.13	1.08	1.06	1.13	1.2	1.17

(1) Data from Liu, Zhai & Liu (2002).
(2) $Ce^*=Ce_N/(La_N^{2/3}\times Nd_N^{1/3})$, $Pr^*=Pr_N/(La_N^{1/3}\times Nd_N^{2/3})$, $TE_1=(Ce^*\times Pr^*)^{1/2}$, $Tb^*=Tb_N/(Gd_N^{2/3}\times Ho_N^{1/3})$, $Dy^*=Dy_N/(Gd_N^{1/3}\times Ho_N^{2/3})$, $TE_3=(Tb^*\times Dy^*)^{1/2}$, $TE_{1,3}=(TE_1{}^*\times TE_3{}^*)^{1/2}$, $Eu^*=Eu_N/(Sm_N\times Gd_N)^{1/2}$.

https://doi.org/10.1017/S0016756807004311 Published online by Cambridge University Press

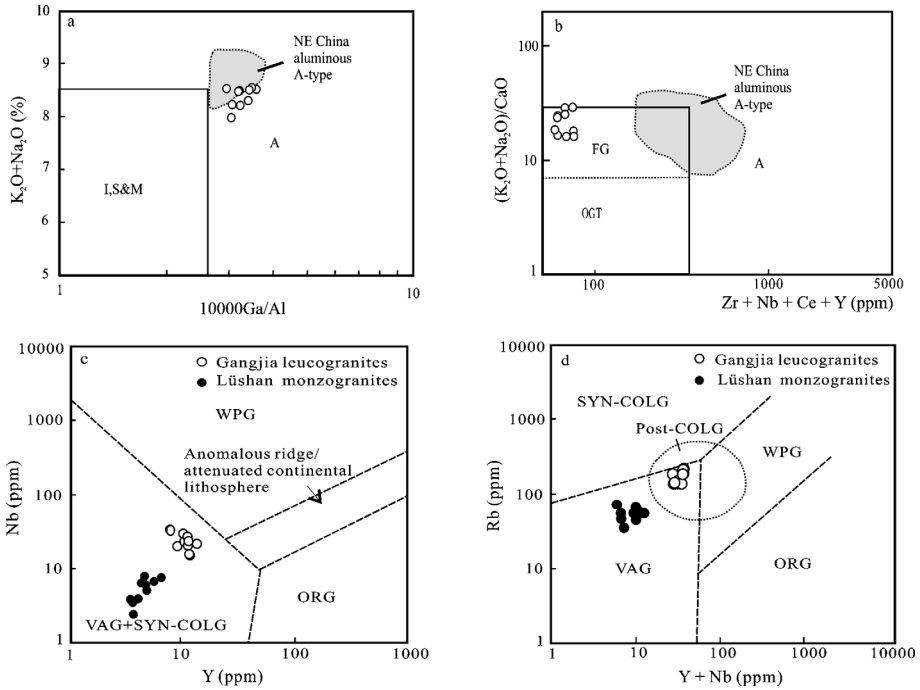

Figure 3. (a) $K_2O + Na_2O$ v. 10 000 Ga/Al and (b) $(K_2O + Na_2O)/CaO$ v. (Zr + Nb + Ce + Y) discrimination diagrams of Whalen, Currie & Chappell (1987), showing both A-type and fractionated nature of the Gangjia granites. OGT – orogenic granite types: unfractionated I- and S-type granites; FG – fractionated felsic I- and S-type granites; (c) Nb v. Y and (d) Rb v. Y + Nb tectonic discrimination diagrams of Pearce, Harris & Tindle (1984). VAG – volcanic arc granites; WPG – within-plate granites; syn-COLG – syn-collisional granites; COLG – collisional granites, ORG – oceanic ridge granites, fields are from Pearce, Harris & Tindle (1984) and post-COLG (post-collisional granites) from Pearce (1996). Data for the Lüshan pluton are from Zhang *et al.* (unpub. data).

6. Discussion

6.a. Petrogenesis

The origin of peraluminous leucogranites has been a subject of much debate. They are generally considered to be formed by partial melting of metasedimentary rocks, mostly as a result of thermal relaxation and/or exhumation of an orogen (e.g. Le Fort, 1981; Chappell & White, 1992; Barbarin, 1996; Nabelek & Bartlett, 1998). However, for those peraluminous leucogranites with the tetrad effect, several workers have proposed that they are highly fractionated products from dominantly mantle-derived parental calc-alkaline magmas (e.g. Jahn *et al.* 2001, 2004*a*; Wu *et al.* 2004).

Chondrite-normalized REE patterns with tetrad effect are characterized by the subdivision into four segments called tetrads (Masuda *et al.* 1987). As briefly reviewed by Jahn *et al.* (2001) and Liu & Zhang (2005), the first documentation of the lanthanide tetrad effect can be traced back to the late 1960s, when two chemists conducted a study of the partitioning of REE between two liquid phases in liquid–liquid extraction (Fidelis & Siekierski, 1966; Peppard, Mason & Lewey, 1969). Since then, tetrad effect-like REE patterns have been successively observed in natural samples from marine and terrestrial geochemical systems (Masuda & Ikeuchi, 1979; Masuda & Akagi, 1989; Lee, Masuda & Kim, 1994; Kawabe, Kitahara & Naito, 1991; Kawabe, 1995; Bau, 1996).

In recent years, discussion about the tetrad effect has focused on highly evolved igneous rocks (Bau, 1996, 1997; Pan, 1997; Irber, 1999; Zhao, Xiong & Han, 1999; Jahn *et al.* 2001, 2004*a*; Wu *et al.* 2004). Since highly evolved granitic rocks are commonly interpreted to represent the transition from a silicate melt to a high-temperature hydrothermal system, the geochemical behaviour of the isovalent incompatible elements in them is controlled mainly by chemical complexation with a variety of ligands (Bau & Dulski, 1995; Bau, 1996, 1997; Dostal & Chatterjee, 2000) and the origin of the REE tetrad effect is thus ascribed to the interaction between fluorine-bearing fluid and silicate melt phases (e.g. Irber, 1999). By now, as well-confirmed by many studies on the REE tetrad effects in the highly evolved magmatic systems and their constituent mineral separates (Zhao, Xiong & Han, 1999; Zhao *et al.* 2002; Jahn *et al.* 2001; Monecke *et al.* 2002; Wu *et al.* 2004; Liu & Zhang, 2005), a consensus has been reached that the tetrad effect and the fractionation between the chemically coherent isovalent elements represent intrinsic features of all highly evolved peraluminous magmatic melts. Moreover, interaction of an external fluid with parent materials of the highly evolved granitic rocks before

https://doi.org/10.1017/S0016756807004311 Published online by Cambridge University Press

Table 3. Rb–Sr and Sm–Nd isotopic compositions for the Gangjia leucogranites

Sample no.	Rb (ppm)	Sr (ppm)	$^{87}Rb/^{86}Sr$	$^{87}Sr/^{86}Sr$	$\pm2\sigma$	$(^{87}Sr/^{86}Sr)_t$	Sm	Nd	$^{147}Sm/^{144}Nd$	$^{143}Nd/^{144}Nd$	$\pm2\sigma$	ε_{Nd} (0)	ε_{Nd} (t)	T_{DM} (Ma)	T_{DM2} (Ma)
FX11-1	150.3	36	12.092	0.734074	14	0.70726	0.17	0.57	0.1809	0.511623	15	−19.8	−19.5	6958	2276
FX11-2	148.7	21	20.514	0.757893	15	0.71240	1.17	3.25	0.2166	0.511662	13	−19.0	−19.4	−110046	2272
FX11-4	166.0	15	31.684	0.773446	25	0.70318	2.30	8.22	0.1694	0.511659	18	−19.1	−18.6	5092	2209
FX11-8	155.7	31	14.582	0.739971	12	0.70763	1.21	3.56	0.2061	0.511648	13	−19.5	−19.3	27576	2276
FX18	200.3	21	28.668	0.774323	19	0.71075	1.72	5.91	0.1766	0.511684	14	−18.6	−18.2	5942	2183
FX20	272.4	22	36.945	0.769354	25	0.68751	0.70	3.99	0.1602	0.511838	17	−15.6	−13.8	1850	1864

Chondrite Uniform Reservoir (CHUR) values ($^{87}Rb/^{86}Sr$=0.0847, $^{87}Sr/^{86}Sr$=0.7045, $^{147}Sm/^{144}Nd$=0.1967, $^{143}Nd/^{144}Nd$=0.512638) are used for the calculation. $\lambda_{Rb}=1.42\times10^{-11}$ yr^{-1} (Steiger & Jäger, 1977); $\lambda_{SM}=6.54\times10^{-12}$ yr^{-1} (Lugmair & Harti, 1978).

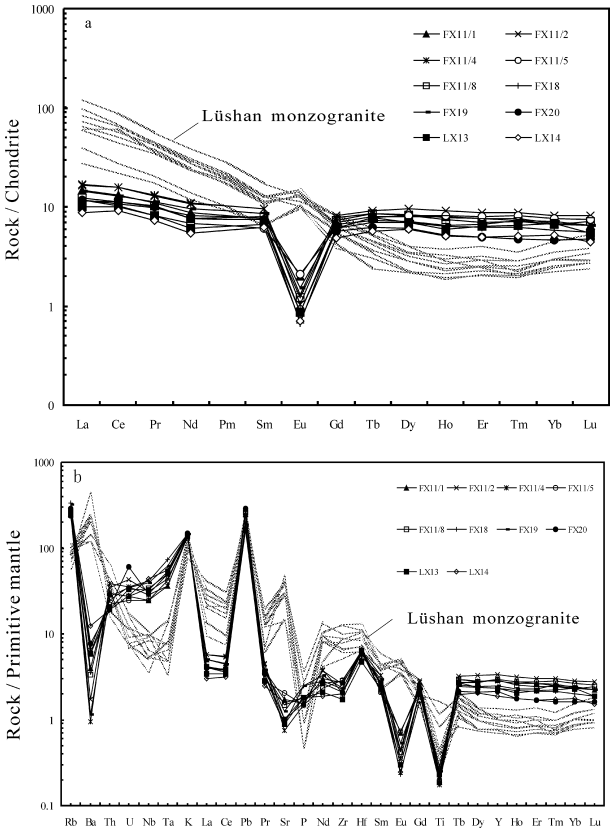

Figure 4. (a) Chondrite-normalized REE patterns and (b) primitive mantle-normalized trace elements spidergram for the Gangjia granites. Data for the Lüshan pluton are from Zhang *et al.* (unpub. data). Normalization values are from Sun & McDonough (1989).

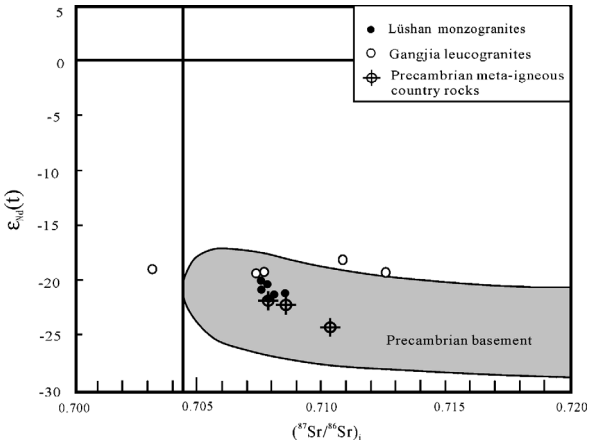

Figure 5. $(^{87}Sr/^{86}Sr)_i$ v. $\varepsilon_{ND}(t)$ plot. Data for the Lüshan pluton and Precambrian meta-igneous rocks are from Zhang *et al.* (unpub. data). Fields for Precambrian basement of the eastern North China craton are after Wu *et al.* (2005*a*).

melting would be favourable for producing the REE tetrad effects in highly evolved granitic rocks (e.g. Liu & Zhang, 2005).

In order to evaluate the degree of the REE tetrad effect and the accompanied non-charge-and-radius-controlled elemental behaviour in the Gangjia granites,

https://doi.org/10.1017/S0016756807004311 Published online by Cambridge University Press

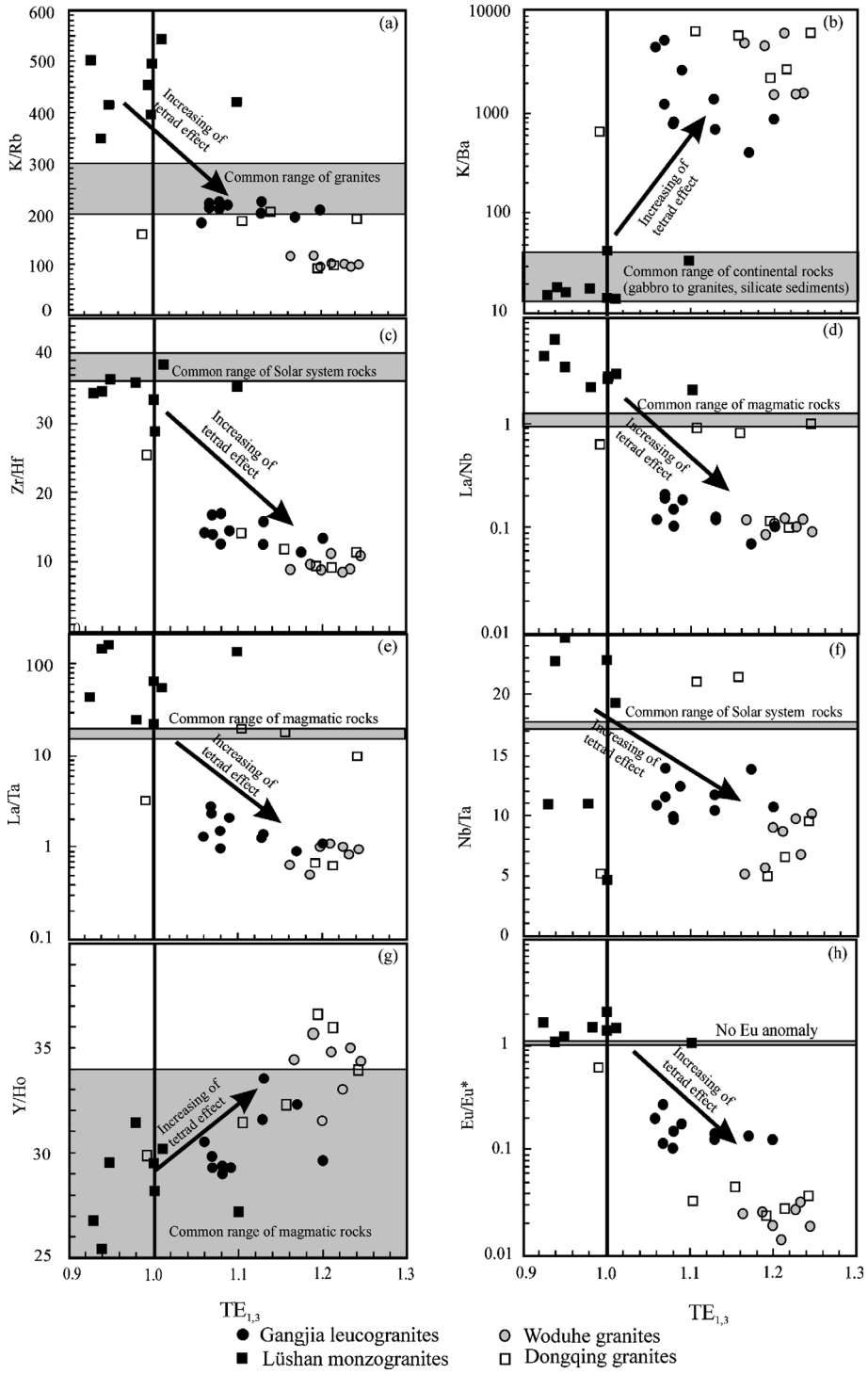

Figure 6. Variation of key elemental ratios as a function of the tetrad effect ($TE_{1,3}$ of Irber, 1999). Reference data for the Woduhe, Dongqing and Lüshan granites are from Jahn *et al.* (2001), Wu *et al.* (2004) and Zhang *et al.* (unpub. data), respectively.

the $TE_{1,3}$ values, the degree of the REE tetrad effect, are plotted versus the geochemically coherent element pairs for the Gangjia samples, together with those from other typical peraluminous leucogranites, such as the Woduhe and Dongqing granites from the Central Asian Orogenic belt (Jahn *et al.* 2001; Wu *et al.* 2004), and those of the monzogranites from the host Lüshan pluton in Figure 6. K/Rb ratios in the Gangjia granites are 178–223, similar to those of the Dongqing granites but lower than the host Lüshan pluton (Fig. 6a), whereas K/Ba ratios are remarkably high (398–5099), similar to those for the Dongqing and Woduhe granites but much higher than those for the host Lüshan pluton (Fig. 6b). For Zr/Hf ratios, which are known to be highly constant at 39 in common granites due to closest geochemical behaviour of Zr and Hf, the Gangjia granites have very

https://doi.org/10.1017/S0016756807004311 Published online by Cambridge University Press

low ratios between 11 and 17 (Fig. 6c). Moreover, as in the case of the Woduhe and Dongqing plutons, the Gangjia granites show much lower La/Nb, La/Ta and Nb/Ta ratios in comparison with common values of magmatic rocks (Fig. 6d, e, f), whereas Y/Ho ratios display little deviation from the common range of magmatic rocks (Fig. 6g). In addition, Eu/Eu* ratios in the Gangjia granites are higher than those for the Dongqing and Woduhe granites but much lower than those for the host Lüshan pluton (Fig. 6h).

These peraluminous granites display generally positive or negative correlations between the $TE_{1,3}$ values and the elemental ratios in Figure 6; the $TE_{1,3}$ values increase with increasing K/Ba and Y/Ho but with decreasing La/Nb, La/Ta, Zr/Hf and Eu/Eu* ratios. This is in good accordance with the general variation trend of the lanthanide tetrad effect degree in the evolution of typical peraluminous magmatic systems (Liu & Zhang, 2005). Therefore, we suggest that the REE tetrad effect and non-charge-and-radius-controlled elemental features developed due to the intense interaction between residual melt and a coexisting aqueous high-temperature fluid.

The existence of an aqueous high-temperature fluid is also indicated by the extremely low Th/U ratios (0.07–0.09) of most of the dated zircons, as the zircons that precipitated from fluid generally have Th/U ratios lower than 0.1 (Hoskin & Schaltegger, 2003). For instance, Rubatto & Hermann (2003) documented a zircon age of 45 ± 1 Ma in an eclogite-facies vein from the Western Alps, with Th/U ratios of 0.01–0.086, much lower than those of host eclogites at 0.1–1.6. They explained that the vein zircons with low Th/U ratios formed from aqueous fluid. Xie, Gao & Chen (2004) also obtained both Triassic and early Cretaceous ages from overgrown zircons with Th/U ratios of lower than 0.1, and they regarded these zircons as genetically related to fluids of uncertain origin. The reason for low Th/U ratios is that U is more soluble than Th and more easily enters fluids (Dobson & Tilton, 1989), which results in fluids with lower Th/U ratios (Xie, Gao & Chen, 2004). In addition, the radius of Th^{4+} is about 4 % greater than that of U^{4+} (Hoskin & Black, 2000), so that it is easier for the latter to enter the crystal lattice, leading to a decrease in the Th/U ratio.

Although the large uncertainties in age-corrected initial $^{87}Sr/^{86}Sr$ values due to high $^{87}Rb/^{86}Sr$ ratios make it difficult to constrain the petrogenesis of the Gangjia granites, the similarity in $\varepsilon_{Nd}(t)$, model ages, age patterns and volcanic arc source material (Fig. 3c, d) between most Gangjia granite samples and the host Lüshan monzogranites, all suggest their comagmatic relationship. For the Lüshan monzogranites, their peraluminous mineralogy, adakite-like trace element signature, low initial Sr isotopic ratios and strongly negative $\varepsilon_{Nd}(t)$ values argue for a felsic magma source that originated from partial melting of ancient meta-igneous lower crust, possibly in response to underplating of mafic mantle-derived magmas (Liu *et al.* 2002). Therefore, the parental magma for the Gangjia granites could be a calc-alkaline magma differentiated from the host Lüshan pluton, as is the case with the Woduhe and Dongqing granites (Jahn *et al.* 2001; Wu *et al.* 2004).

6.b. Tectonic implications

Given the highly differentiated nature of the Gangjia granites, it is difficult to classify them. The reasons may be twofold: on one hand, their highly differentiated character obliterates many geochemical signatures possibly related to a particular source rock or tectonic setting. On the other hand, there is no *a priori* reason that would restrict any particular granitoid type to any particular tectonic environment, as pointed out by Frost *et al.* (2001). However, with the REE tetrad effect as the intrinsic feature of all highly evolved peraluminous magmatic melts and the indicator for interaction of an external fluid with the parental magma or the parental materials before melting, the physiochemical conditions necessary for their genesis are by no means ubiquitous in the tectonic evolution of an orogenic belt. They are generally related to post-orogenic extensional regimes, as evidenced by the general features of post-orogenic and anorogenic magmatism (e.g. Liégeois, 1998; Bonin, 2004) and specific examples worldwide (Sibel, Hohndorf & Wendt, 1995; Williamson *et al.* 1996; Förster *et al.* 1999; Monecke *et al.* 2002; Jahn *et al.* 2001, 2004*a*; Wu *et al.* 2004; Sun *et al.* 2005). For instance, the two-mica leucogranites from the Massif Central in France are considered to be formed during Hercynian extensional orogenic collapse (Williamson *et al.* 1996). The peraluminous leucogranites in the Variscan Erzgebirge of Germany were associated with extension during post-orogenic collapse (Förster *et al.* 1999). The Mesozoic peraluminous leucogranites from the Central Asian Orogenic belt, as represented by the early Cretaceous Woduhe and Ongonites granites (Jahn *et al.* 2001, 2004a) and the Jurassic Dongqing granites (Wu *et al.* 2004), are emplaced in post-orogenic and intra-continental settings (Wu *et al.* 2002; Jahn *et al.* 2004*b*).

Therefore, it seems that peraluminous leucogranites with the REE tetrad effect can take on a distinctive tectonic implication for post-orogenic or intra-continental extensional settings. It is not by accident that most of such peraluminous leucogranites plot in the field of A-type granites in the geochemical discriminant diagram of Whalen, Currie & Chappell (1987), since many A-type granites are also inherently highly fractionated and display characteristic REE tetrad patterns (e.g. Wu *et al.* 2002; Chen & Jahn, 2004; Liu *et al.* 2005).

In our case, as stated above, Western Liaoning experienced the most voluminous magmatism during middle to late Jurassic times. However, it is still not certain what caused this prolonged magmatism.

https://doi.org/10.1017/S0016756807004311 Published online by Cambridge University Press

Consistent with the prevalent dual geodynamic models put forward for the Mesozoic magmatism in Eastern China (Wu *et al.* 2005*a*, and references therein), some authors advocate post-collisional magmatism developed in an intra-continental extensional regime (Liu, Zhai & Liu, 2002; Zhang *et al.* 2003), while others relate the events to the subduction of the palaeo-Pacific slab (Wu *et al.* 2005*a*; Wu, Yang & Zhang, 2006).

For all such uncertainty, it is the thermal regime and source rocks that played an essential role in determining the chemical and petrological characteristics of granites. For the Mesozoic tectono-thermal state of the North China craton, a well-established consensus is that considerable lithospheric thinning took place beneath the eastern North China craton (Menzies, Fan & Zhang, 1993; O'Reilly *et al.* 2001; Zhang *et al.* 2003). Extensive Mesozoic magmatism, large-scale basin formation and the development of metamorphic core complexes in eastern North China craton were commonly considered to be related to the lithospheric mantle removal which most likely took place during Jurassic–Cretaceous time (Gao *et al.* 2002, 2004; Wilde *et al.* 2003). These typical mantle and crustal signatures also attest to a prevalent intraplate extensional tectonic regime for the Early Cretaceous in the Yanshan belt (Meng, 2003) and Eastern China (e.g. Wu *et al.* 2005*b*).

As reviewed by various authors (e.g. Liegeois, 1998; Vanderhaeghe & Teyssier, 2001; Bonin, 2004), an orogenic cycle generally comprises a pre-collisional period characterized by subduction leading to oceanic basin closure and terrane docking, a period of arc–continent or continent–continent collision accommodated by crustal thickening and post-collisional to post-orogenic periods. Corresponding to the successive collision, post-collisional, post-orogenic and within-plate settings, four stages of mantle unrooting process are identified, including orogenic growth, initiation of gravitational instability until lithospheric failure, sinking of the detached lithosphere and relaxation of the system (Marotta, Fernandez & Sabadini, 1998; Bonin, 2004). Based on the comparison of the first-order features displayed by various orogenic belts, Vanderhaeghe & Teyssier (2001) also suggest that the thermal and mechanical evolution of the continental crust during an orogenic cycle can be generalized into such stages as crustal thickening, thermal maturation, partial melting, and syn- to post-convergence gravitational collapse.

When evaluated within the context of this general thermal and mechanical evolution of the continental crust during orogenesis, the Yanshan orogen-scale features of both mantle and crustal levels during the early Cretaceous are typical of lithospheric and crustal signatures at the very end of the post-collisional stage (Bonin, 2004), corresponding to the third stage, that is, sinking of the detached lithosphere, in terms of mantle unrooting process (Marotta, Fernandez & Sabadini, 1998). Therefore, we suggest that the Yanshan belt might be in a post-collisional geodynamic setting associated with the northern Solonker and Mongol–Okhotsk sutures in the Jurassic, with a corresponding mantle unrooting process as characterized by lithospheric stacking and initiated gravitational instability (Bonin, 2004). This agrees with the conclusion reached by recent *in situ* U–Pb dating and Hf isotopic analyses on detrital zircons from Palaeozoic to Late Mesozoic strata in the Xishan west of Beijing, which states that the Yanshan belt experienced a rapid uplift from 205 to 158 Ma under a transitional geodynamic setting from a post-collisional to an intraplate extensional setting (Yang *et al.* 2006).

Under such a post-orogenic tectonic regime favourable for producing Chinese C-type (high potassium) adakites (Xiao & Clemens, 2006), upwelling of hot asthenosphere due to lithospheric removal caused mantle-derived magma underplating and partial melting of ancient lower crust (Gao *et al.* 2004; Wang *et al.* 2007). This subsequently led to the formation of voluminous Mesozoic adakitic magmatism in the eastern North China craton (Jiang *et al.* 2007), and more specifically, the voluminous Jurassic adakite-like magmatism as represented by Lüshan pluton in Western Liaoning (Liu *et al.* 2002). Given the consistent occurrences of peraluminous leucogranites with the REE tetrad effect under post-orogenic extensional settings, our documentation of such distinctive peraluminous magmatism as represented by the Gangjia leucogranites in Yiwulüshan provides further diagnostic constraints for supporting a post-orogenic extensional tectonic regime for the Jurassic magmatism in Western Liaoning. At the very end of this prolonged magmatic evolution, extensive fractionation of most probably ferromagnesian phases and plagioclase from a calc-alkaline magma parental to the host Lüshan pluton, with overprint of the magmatic hydrothermal fluid, produced highly evolved peraluminous parental magmas for the Gangjia granites.

7. Conclusions

SHRIMP U–Pb zircon dating and geochemical analyses document an episode of late Jurassic peraluminous magmatism in Yiwulüshan in western Liaoning Province, North China craton. The peculiar geochemical characteristics, including REE tetrad effect, non-charge-and-radius-controlled trace element behaviour and zircons with low Th/U ratios, suggest an origin that is consistent with the interaction between a residual melt and coexisting high-temperature aqueous fluid. The similarity in $\varepsilon_{Nd}(t)$, model ages and age patterns between the Gangjia granites and the host Lüshan pluton and their common volcanic arc signature in source material indicate their comagmatic nature. The first documentation of such unusual peraluminous magmatism in Western Liaoning provides an exceptional hallmark for indicating that the prolonged

https://doi.org/10.1017/S0016756807004311 Published online by Cambridge University Press

Jurassic magmatism most likely took place under a post-orogenic extensional tectonic regime. Extensive fractionation from a calc-alkaline magma parental to the host Lüshan pluton, coupled with the magmatic hydrothermal fluid, led to the formation of the highly evolved peraluminous parental magmas for the Gangjia granites.

Acknowledgements. This study was financially supported by the Knowledge Innovation Program of the Chinese Academy of Sciences (Grant no. KZCX2-YW-103), the National Natural Science Foundation of China (Grant no. 40534022) and the Major State Basic Research Program of the People's Republic of China (Grant no. 2006CB403504). The authors thank Mr Z. Q. Yang for help in U–Pb analyses, Mr H. Li and Ms X. D. Jin in major- and trace-element analysis, Dr Z. Y. Chu in Sr–Nd isotope analyses. We are also grateful to Dr D. Pyle and two anonymous reviews for their constructive suggestions and Mrs J. Holland for editorial handling. This is The Institute for Geoscience Research (TIGeR) publication no. 64.

References

BARBARIN, B. 1996. Genesis of the two main types of peraluminous granitoids. *Geology* **24**, 295–8.

BARBARIN, B. 1999. A review of the relationships between granitoid types, their origins and their geodynamic environments. *Lithos* **46**, 605–26.

BAU, M. 1996. Controls on the fractionation of isovalent trace elements in magmatic and aqueous systems: evidence from Y/Ho, Zr/Hf, and lanthanide tetrad effect. *Contributions to Mineralogy and Petrology* **123**, 323–33.

BAU, M. 1997. The Lanthanide tetrad effect in highly evolved felsic igneous rocks – a reply to the comment by Y. Pan. *Contributions to Mineralogy and Petrology* **128**, 409–12.

BAU, M. & DULSKI, P. 1995. Comparative study of yttrium and rare-earth element behaviors in fluorine-rich hydrothermal fluids. *Contributions to Mineralogy and Petrology* **119**, 213–23.

BLACK, L. P., KAMO, S. L., ALEIIKOFF, J. N., DAVIS, D. W., KORSCH, R. L. & FOUDOULIS, C. 2003. TEMORA 1: a new zircon standard for Phanerozoic U–Pb geochronology. *Chemical Geology* **200**, 155–70.

BONIN, B. 2004. Do coeval mafic and felsic magmas in post-collisional to within-plate regimes necessarily imply two contrasting mantle and crustal sources? A review. *Lithos* **78**, 1–24.

BUCHAN, C., PFÄNDER, J., KRÖNER, A., BREWER, T. S., TOMURTOGOO, O., TOMURHUU, D., CUNNINGHAM, D. & WINDLEY, B. F. 2002. Timing of accretion and collisional deformation in the Central Asian Orogenic Belt: Implications of granite geochronology in the Bayankhongor ophiolite zone. *Chemical Geology* **192**, 23–45.

CHAPPELL, B. W. & WHITE, A. J. R. 1992. I- and S-type granites in the Lachlan Fold Belt. *Transactions of Royal Society of Edinburgh: Earth Sciences* **83**, 1–26.

CHEN, B. & JAHN, B. M. 2004. Genesis of post-collisional granitoids and basement nature of the Junggar Terane, NW China: Nd–Sr isotope and trace element evidence. *Journal of Asian Earth Sciences* **23**, 691–703.

COMPSTON, W., WILLIAMS, I. S., KIRSCHIVINK, J. L., ZHANG, Z. & MA, G. 1992. Zircon U–Pb ages for the early Cambrian time-scale. *Journal of the Geological Society, London* **149**, 171–84.

DARBY, B. J., DAVIS, G. A., ZHANG, X. H., WU, F. Y., WILDE, S. A. & YANG, J. H. 2004. The newly discovered Waziyu metamorphic core complex, Yiwulüshan, western Liaoning province, North China. *Earth Science Frontiers* **11**, 145–55.

DAVIS, G. A., XU, B., ZHENG, Y. & ZHANG, W. 2004. Indosinian extension in the Solonker suture zone: the Sonid Zuoqi metamorphic core complex, Inner Mongolia, China. *Earth Science Frontiers* **11**, 135–43.

DAVIS, G. A., WANG, C., ZHENG, Y. D., ZHANG, J. J., ZHANG, C. & GEHRELS, G. E. 1998. The enigmatic Yinshan fold and thrust belt of northern China: New views on its intraplate contractional styles. *Geology* **26**, 43–6.

DAVIS, G. A., ZHENG, Y., WANG, C., DARBY, B. J., ZHANG, C. & GEHRELS, G. E. 2001. Mesozoic tectonic evolution of the Yanshan fold and thrust belt, with emphasis on Hebei and Liaoning provinces, northern China. In *Paleozoic and Mesozoic tectonic evolution of central and eastern Asia: From continental assembly to intracontinental deformation* (eds M. S. Hendrix & G. A. Davis), pp. 171–97. Geological Society of America, Memoir no. 194.

DOBSON, P. F. & TILTON, G. R. 1989. Th, U and Pb systematics of boninite series volcanic rocks from Chichi-jima, Bonin Islands, Japan. In *Boninites* (ed. A. J. Crawford), pp. 396–415. Cambridge University Press.

DOSTAL, J. & CHATTERJEE, A. K. 2000. Contrasting behavior of Nb/Ta and Zr/Hf ratios in a peraluminous granitic pluton (Nova Scotia, Canada). *Chemical Geology* **163**, 207–18.

FIDELIS, I. & SIEKIERSKI, S. 1966. The regularities in stability constants of some rare earth complexes. *Journal of Inorganic and Nuclear Chemistry* **28**, 185–8.

FÖRSTER, H. J., TISCHENDORF, G., TRUMBULL, R. B. & GOTTESMANN, B. 1999. Late-collisional granites in the Variscan Erzgebirge, Germany. *Journal of Petrology* **40**, 1613–45.

FROST, B. R., BARNES, C. G., COLLINS, W. J., ARCULUS, R. J., ELLIS, D. J. & FROST, C. D. 2001. A geochemical classification for granitic rocks. *Journal of Petrology* **42**, 2033–48.

GAO, S., RUDNICK, R. L., CARLSON, R. W., MCDONOUGH, W. F. & LIU, Y. S. 2002. Re–Os evidence for replacement of ancient mantle lithosphere beneath the North China craton. *Earth and Planetary Science Letters* **198**, 307–22.

GAO, S., RUDNICK, R. L., YUAN, H. L., LIU, X. M., LIU, Y. S., XU, W. L., AYERS, J., WANG, X. C. & WANG, Q. H. 2004. Recycling lower continental crust in the North China craton. *Nature* **432**, 892–7.

HOSKIN, P. W. O. & BLACK, L. P. 2000. Metamorphic zircon formation by solid-state recrystallization of protolith igneous zircon. *Journal of Metamorphic Geology* **18**, 423–39.

HOSKIN, P. W. O. & SCHALTEGGER, U. 2003. The composition of zircon and igneous and metamorphic petrogenesis. In *Zircon* (eds J. M. Hanchar & P. W. O. Hoskin), pp. 27–62. Reviews in Mineralogy & Geochemistry, no. 53.

IRBER, W. 1999. The lanthanide tetrad effect and its correlation with K/Rb, Eu/Eu*, Sr/Eu, Y/Ho, and Zr/Hf of evolving peraluminous granite suites. *Geochimica et Cosmochimica Acta* **63**, 489–508.

JAHN, B. M., CAPDEVIA, R., LIU, D., VERNON, A. & BADARCH, G. 2004*a*. Sources of Phanerozoic granitoids in the transect Bayanhongor–Ulaan Baatar, Mongolia: geochemical and Nd isotopic evidence, and implications for Phanerozoic crustal growth. *Journal of Asian Earth Sciences* **23**, 604–53.

JAHN, B. M., WINDLEY, B., NATAL'IN, B. & DOBRETSOV, N. 2004*b*. Phanerozoic continental growth in Central Asia. *Journal of Asian Earth Sciences* **23**, 599–603.

JAHN, B. M., WU, F., CAPDEVILA, R., MARTINEAU, F., ZHAO, Z. & WANG, Y. 2001. Highly evolved juvenile granites with tetrad REE patterns: the Wudohe and Baerzhe granites from the Great Xing'an Mountains in NE China. *Geochimica et Cosmochimica Acta* **59**, 171–98.

JIANG, N., LIU, Y. S., ZHOU, W. G., YANG, J. H. & ZHANG, S. Q. 2007. Derivation of Mesozoic adakitic magmas from ancient lower crust in the North China craton. *Geochimica et Cosmochimica Acta* **71**, 2591–608.

KAWABE, I. 1995. Tetrad effects and fine structures of REE abundance patterns of granitic and rhyolitic rocks: ICP-AES determinations of REE and Y in eight GSJ reference rocks. *Geochemical Journal* **29**, 213–30.

KAWABE, I., KITAHARA, Y. & NAITO, K. 1991. Non-chondritic yttrium/holmium ratio and lanthanide tetrad effect observed in pre-Cenozoic limestones. *Geochemical Journal* **25**, 31–4.

LE FORT, P. 1981. Manaslu leucogranite: A collision signature of the Himalaya, a model for its genesis and emplacement. *Journal of Geophysical Research* **86**, 10545–68.

LEE, S. G., MASUDA, A. & KIM, H. S. 1994. An early Proterozoic leucogranitic gneiss with the REE tetrad phenomenon. *Chemical Geology* **114**, 59–67.

LIAONING BUREAU OF GEOLOGY AND MINERAL RESOURCES (LBGMR). 1998. *1:50000 scale regional geology of Badaohao and related maps*, *Liaoning Province* (in Chinese).

LIÉGEOIS, J. 1998. Preface – some words on the post-collisional magmatism. *Lithos* **45**, xv–xvii.

LIU, C. & ZHANG, H. 2005. The lanthanide tetrad effect in apatite from the Altay No. 3 pegmatite, Xinjiang, China: an intrinsic feature of the pegmatite magma. *Chemical Geology* **214**, 61–77.

LIU, D., NUTMAN, A. P., COMPSTON, W., WU, J. & SHEN, Q. 1992. Remnants of ≥ 3800 Ma crust in the Chinese part of the Sino-Korean craton. *Geology* **20**, 339–42.

LIU, H., SUN, S., LIU, J. & ZHAI, M. 2002. The Mesozoic high-Sr granitoids in the northern marginal region of North China craton: geochemistry and source region. *Acta Petrologica Sinica* **18**, 257–74 (in Chinese with English abstract).

LIU, H., ZHAI, M. & LIU, J. 2002. The Mesozoic granitoids in the northern marginal region of North China craton: evolution from post-collisional to anorogenic settings. *Acta Petrologica Sinica* **18**, 433–48 (in Chinese with English abstract).

LIU, W., SIEBEL, W., LI, X. & PAN, X. 2005. Petrogenesis of the Linxi granitoids, northern Inner Mongolia of China: constraints on basaltic underplating. *Chemical Geology* **219**, 3–35.

LUDWIG, K. 2001. *User manual for Isoplot/EX (2.49)*. Berkeley Geochronology Center, Special Publication no. 1a. 55 pp.

LUGMAIR, G. W. & HARTI, K. 1978. Lunar initial $^{143}Nd/^{144}Nd$: differential evolution of the lunar crust and mantle. *Earth and Planetary Science Letters* **39**, 349–57.

MAROTTA, A. M., FERNANDEZ, M. & SABADINI, R. 1998. Mantle unrooting in collisional setting. *Tectonophysics* **296**, 31–46.

MASUDA, A. & AKAGI, T. 1989. Lanthanide tetrad effect observed in leucogranites from China. *Geochemical Journal* **23**, 245–53.

MASUDA, A. & IKEUCHI, Y. 1979. Lanthanide tetrad effects observed in marine environment. *Geochemical Journal* **13**, 19–22.

MASUDA, A., KAWAKAMI, O., DOHMOTO, Y. & TAKENAKA, T. 1987. Lanthanide tetrad effects in nature: two mutually opposite type W and M. *Geochemical Journal* **21**, 119–24.

MENG, Q. 2003. What drove late Mesozoic extension of the northern China–Mongolia tract? *Tectonophysics* **389**, 155–74.

MENG, Q. & ZHANG, G. 2000. Geological framework and tectonic evolution of Qinling orogen, central China. *Tectonophysics* **323**, 183–96.

MENZIES, M. A., FAN, W. M. & ZHANG, M. 1993. Palaeozoic and Cenozoic lithoprobes and the loss of >120 km of Archean lithosphere, Sino-Korean craton, China. In *Magmatic Processes and Plate Tectonics* (eds H. M. Prichard, T. Alabaster, N. B. W. Harris & C. R. Neary), pp. 71–81. Geological Society of London, Special Publication no. 76.

MONECKE, T., KEMPE, U., MONECKE, J., SALA, M. & WOLF, D. 2002. Tetrad effect in rare earth element distribution patterns: a method of quantification with application to rock and mineral sample from granite-related rare metal deposits. *Geochimica et Cosmochimica Acta* **66**, 1185–96.

NABELEK, P. & BARTLETT, C. 1998. Petrologic and geochemical links between the post-collisional Proterozoic Harney Peak leucogranite, south Dakota, USA, and its source rocks. *Lithos* **45**, 71–85.

O'REILLY, S. Y., GRIFFIN, W. L., POUDJOM DJOMANI, Y. H. & MORGAN, P. 2001. Are lithospheres forever? Tracking changes in sub-continental lithospheric mantle through time. *GSA Today* **11**, 4–10.

PAN, Y. 1997. Controls on the fractionation of isovalent trace elements in magmatic and aqueous systems: evidence fro Y/Ho, Zr/Hf, and lanthanide tetrad effect – A discussion of the article by M. Bau (1996). *Contributions to Mineralogy and Petrology* **128**, 405–8.

PEARCE, J. A. 1996. Sources and settings of granitic rocks. *Episodes* **19**, 120–5.

PEARCE, R. R., HARRIS, N. B. W. & TINDLE, A. G. 1984. Trace element discrimination diagrams for the tectonic interpretation of granitic rocks. *Journal of Petrology* **25**, 956–83.

PEPPARD, D. F., MASON, G. W. & LEWEY, S. 1969. A tetrad effect in liquid extraction ordering of lanthanide (III). *Journal of Inorganic and Nuclear Chemistry* **31**, 339–43.

RITTS, B. D., DARBY, B. J. & COPE, T. 2001. Early Jurassic extensional basin formation in the Daqingshan segment of the Yinshan belt, northern North China, Inner Mongola. *Tectonophysics* **339**, 239–58.

RUBATTO, D. & HERMANN, J. 2003. Zircon formation during fluid circulation in eclogites (Monviso, Western Alps): Implication for Zr and Hf budget in subduction

zones. *Geochimica et Cosmochimica Acta* **67**, 2173–87.

SIBEL, W., HOHNDORF, A. & WENDT, I. 1995. Origin of late Variscan granitoids from NE Bavaria, exemplified by REE and Nd isotope systematics. *Chemical Geology* **125**, 249–70.

STEIGER, R. H. & JÄGER, E. 1977. Subcommission on geochronology; convention on the use of decay constants in geochronology and cosmochronology. *Earth and Planetary Science Letters* **36**, 359–62.

SUN, S. S. & MCDONOUGH, W. F. 1989. Chemical and isotopic systematics of oceanic basalts: implications for mantle composition and processes. In *Magmatism in the Ocean Basins* (eds A. D. Saunders & M. J. Norry), pp. 528–48. Geological Society of London, Special Publication no. 42.

SUN, T., ZHOU, X., CHEN, P., LI, H., ZHOU, H., WANG, Z. & SHEN, W. 2005. Strongly peraluminous granites of Mesozoic in Eastern Nanling Range, southern China: Petrogenesis and implications for tectonics. *Science in China (series D)* **48**, 165–74.

VANDERHAEGHE, O. & TEYSSIER, C. 2001. Partial melting and flow of orogens. *Tectonophysics* **342**, 451–72.

WANG, H. & MO, X. 1995. An outline of tectonic evolution of China. *Episodes* **18**, 6–16.

WANG, Z. H., ZHAO, Y., ZOU, H. B., LI, W. P., LIU, X. W., WU, H., XU, G. & ZHANG, S. 2007. Petrogenesis of the Early Jurassic Nandaling flood basalts in the Yanshan belt, North China craton: A correlation between magmatic underplating and lithosperic thinning. *Lithos* **96**, 543–66.

WHALEN, J. B., CURRIE, K. L. & CHAPPELL, B. W. 1987. A-type granites: geochemical characteristics, discrimination and petrogenesis. *Contributions to Mineralogy and Petrology* **95**, 407–19.

WILDE, S. A., ZHOU, X., NEMCHIN, A. A. & SUN, M. 2003. Mesozoic crust–mantle interaction beneath the North China craton: A consequence of the dispersal of Gondwanaland and accretion of Asia. *Geology* **31**, 817–20.

WILLIAMS, I. S. 1998. U–Th–Pb geochronology by ion microprobe. In *Applications of microanalytical techniques to understanding mineralizaing processes* (eds M. A. Mckinbben, W. C. Shanks III & W. I. Ridey) pp. 1–35. Reviews in Economic Geology, no. 7.

WILLIAMSON, B. J., SHAW, A., DOWNES, H. & THIRLWALL, M. F. 1996. Geochemical constraints on the genesis of Hercynian two-mica leucogranites from the Massif Central France. *Chemical Geology* **127**, 25–42.

WU, F. Y., JAHN, B. M., WILDE, S. A., ZHANG, X. O. & YANG, J. H. 2005*b*. *Nature* and significance of the early Cretaceous giant igneous event in eastern China. *Earth and Planetary Science Letters* **233**, 103–19.

WU, F. Y., SUN, D., JAHN, B. M. & WILDE, S. A. 2004. A Jurassic garnet-bearing granitic pluton from NE China showing tetrad REE patterns. *Journal of Asian Earth Sciences* **23**, 731–44.

WU, F. Y., SUN, D. Y., LI, H. M., JAHN, B. M. & WILDE, S. A. 2002. A-type granites in northeastern China: age and geochemical constraints on their petrogenesis. *Chemical Geology* **187**, 143–73.

WU, F. Y., YANG, J. H., WILDE, S. A. & ZHANG, X. O. 2005*a*. Geochronology, petrogenesis and tectonic implications of Jurassic granites in the Liaodong peninsula, NE China. *Chemical Geology* **221**, 127–56.

WU, F. Y., YANG, J. H. & ZHANG, Y. B. 2006. Emplacement ages of the Mesozoic granites in southeastern part of the the Western Liaoning province. *Acta Petrologica Sinica* **22**, 315–25 (in Chinese with English abstract).

XIAO, L. & CLEMENS, J. D. 2006. Origin of potassic (C-type) adakite magmas: Experimental and field constraints. *Lithos* **95**, 399–414.

XIAO, W., WINDLEY, B. F., HAO, J. & ZHAI, M. 2003. Accretion leading to collision and the Permian Solonker suture, Inner Mongolia, China: Termination of the central Asian orogenic belt. *Tectonics* **22**, 1069, 8.1–8.21.

XIE, Z., GAO, T. & CHEN, J. 2004. Multi-stage evolution of gneiss from North Dabie: evidence from zircon U–Pb chronology. *Chinese Science Bulletin* **49**, 1963–9.

XU, M., MIDDLETON, M. F., XUE, L. F. & WANG, D. P. 2000. Structure of the Lithosphere and Mesozoic sedimentary basins in Western Liaoning, Northern Liaoning, and Songliao, Northeast China. *International Geology Review* **42**, 269–78.

YAN, G., MU, B., XU, B., HE, G., TAN, L., ZHAO, H. & HE, Z. 2000. Geochronology and isotopic features of Sr, Nd, and Pb of the Triassic alkali intrusions in the Yanshan–Yinshan regions. *Science in China (series D)* **30**, 384–7.

YANG, J. H., WU, F. Y., SHAO, J. A., WILDE, S. A., XIE, L. W. & LIU, X. M. 2006. Constraints on the timing of uplift of the Yanshan fold and thrust belt, North China Craton. *Earth and Planetary Science Letters* **246**, 336–52.

YIN, A. & NIE, S. 1996. A Phanerozoic palinspastic reconstruction of China and its neighboring regions. In *Tectonic Evolution of Asia* (eds A. Yin & T. M. Harrison), pp. 442–85. Cambridge University Press.

ZHANG, C., WANG, G., WANG, G., WU, Z., ZHANG, L. & SUN, W. 2002. Thrust tectonics in the eastern segment of the intraplate Yanshan orogenic belt, western Liaoning province, north China. *Acta Geologica Sinica* **76**, 64–76 (in Chinese with English abstract).

ZHANG, H. F., SUN, M., ZHOU, X. H., ZHOU, M. F., FAN, W. M. & ZHENG, J. P. 2003. Secular evolution of the lithosphere beneath the eastern North China craton: Evidence from Mesozoic basalts and high-Mg andesites. *Geochimica et Cosmochimica Acta* **67**, 4373–87.

ZHANG, X. H., LIU, H. T., ZHANG, H. F. & WILDE, S. A. 2008. Jurassic intrusive complexes from Yiwulüshan, western Liaoning, North China craton: geochronology, petrogenesis and tectonic implications. *Contributions to Mineralogy and Petrology* (in press).

ZHANG, X. H., WANG, H. & MA, Y. J. 2003. $^{40}Ar/^{39}Ar$ age constraints on two NNE-trending ductile shear zones from Yanshan orogen, North China craton. *International Geology Reviews* **45**, 936–47.

ZHAO, G. C., SUN, M., WILDE, S. A. & LI, S. Z. 2005. Late Archean to Paleoproterozoic evolution of the North China craton: key issues revisited. *Precambrian Research* **136**, 177–202.

ZHAO, G. C., WILDE, S. A., CAWOOD, P. A. & SUN, M. 2001. Archean blocks and their boundaries in the North China craton: lithological, geochemical, structural and P–T path constraints and tectonic evolution. *Precambrian Research* **107**, 45–73.

ZHAO, Z., XIONG, X. & HAN, X. 1999. The formation mechanism of REE tetrad in granites. *Science in China (Series D)* **29**, 331–8 (in Chinese).

https://doi.org/10.1017/S0016756807004311 Published online by Cambridge University Press

ZHAO, Z., XIONG, X., HAN, X., WANG, Y., WANG, Q., BAO, Z. & JAHN, B. 2002. Controls on the REE tetrad effect in granites: evidence from the Qianlishan and Baerzhe granites, China. *Geochemical Journal* **36**, 527–43.

ZHENG, J. P., GRIFFIN, W. L., O'REILLY, S. Y., LU, F. X., WANG, C. Y., ZHANG, M., WANG, F. Z. & LI, H. M. 2004. 3.6 Ga lower crust in central China: new evidence on the assembly of the North China craton. *Geology* **32**, 229–32.

ZORIN, Y. A. 1999. Geodynamics of the western part of the Mongolia–Okhostk collisional belt, Trans-Baikal region (Russia) and Mongolia. *Tectonophysics* **306**, 33–56.

https://doi.org/10.1017/S0016756807004311 Published online by Cambridge University Press